Modified PI Controller with Improved Steady-State Performance and Comparison with PR Controller for Direct Matrix Converters

Jianwei Zhang [1, 2*], *Li Li* [2], *David G. Dorrell* [3], *Youguang Guo* [2]
(1. College of Electric Power, Inner Mongolia University of Technology, Hohhot, China;
2. Faculty of Engineering and IT, University of Technology Sydney, Sydney, Australia;
3. Howard College Campus, University of KwaZulu-Natal, Durban, South Africa)

Abstract: A modified proportional integral (PI) controller is proposed and compared with a proportional resonant (PR) controller. These controllers are tested on a three-phase direct matrix converter (MC). The modified PI controller employs current feedforward together with space vector modulation to control MC output currents. Compared with the PR controller, the modified PI controller provides increased control flexibility for reducing current error, as well as improved steady-state tracking performance. When the coefficient of current feedforward is equal to load resistance ($K = R$), steady-state error is effectively minimized even when sinusoidal variables are regulated. Additionally, total harmonic distortion is reduced. To comparatively evaluate the modified PI controller, a PR controller is designed and tested. Both the modified PI and PR controllers are implemented in a natural frame (*abc*) in a straightforward manner. This removes the coordinate transformations that are required in stationary ($\alpha\beta$) and synchronous (*dq*) reference frame-based control strategies. Additionally, both controllers can handle unbalanced conditions. The experimental and simulation results verify the feasibility and effectiveness of the proposed controller.

Keywords: Matrix Converter; AC/AC Conversion; Steady-State Error; PI Controller; PR Controller

I. INTRODUCTION

The three-phase direct matrix converter (MC) shown in Fig. 1 is an alternative solution for alternating-current (AC)/AC conversion. It has several key features, such as a compact structure, a bidirectional power flow, sinusoidal waveforms, and a controllable input power factor [1–3]. MCs have been proposed for various applications [4–7]. In industry, manufacturers such as Yaskawa [8, 9], Eupec [1, 10] and Fuji [11] have produced MC products, e.g., the Yaskawa U1000, AC7, Eupec ECONOMAC FM35R12KE3ENG, and Fuji FRENIC-MX1S. The power ratings of the Yaskawa MX1S series MC have reached 6.3 MVA [12].

In the literature, various control strategies have been proposed for MCs [3]. However, many are either too complex or impractical to implement. Model predictive control is a widely researched strategy; however, it is not practical for MCs, because of the large number of switch actions. Space vector modulation (SVM) is a well-developed and common control technique for MCs; however, it is ineffective when the load is unknown, because the output current is required for the modulation. Therefore, the development of closed-loop SVM is important.

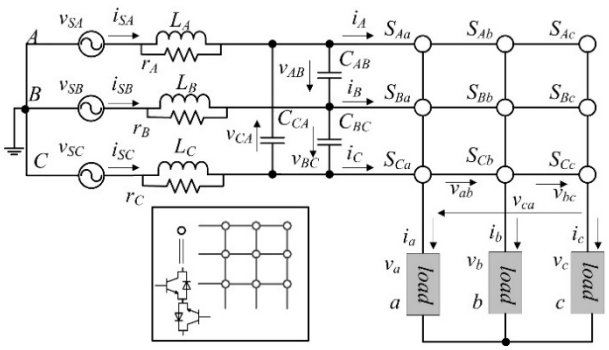

Fig. 1. Three-phase direct MC.

To form the closed loop, proportional–integral (PI) controllers can be employed, as they are simple and easy to implement. This approach has been widely used in power electronic converters and other industrial applications [13, 14]. PI controllers, when used in a power electronic converter, typically adopt one of the following three reference frames: the synchronous reference frame (*dq*), stationary reference frame ($\alpha\beta$), or natural frame (*abc*) [4]. Both $\alpha\beta$ and *dq* frame-based strategies require multiple frame transformations, increasing the complexity and the difficulty

*Corresponding Author, Email: Jianwei Zhang, zjwzachary@outlook.com

of signal processing and implementation. Stationary-frame PI controllers are considered unsatisfactory owing to their significant steady-state errors, particularly for tracking AC variables. This is because stationary controllers offer a limited gain at nonzero frequencies [5, 15, 16].

In contrast, synchronous PI controllers are commonly used because they can achieve zero steady-state error owing to the infinite gain of the direct-current (DC) signal provided by the integral term. However, the synchronous-frame controller is more complex than the stationary-frame controller because several transformations are needed (*abc*↔*dq*) to convert the controlled signals into DC quantities. The controllers are error-prone because of the noise in the synchronous reference-signal detection, which can introduce extra errors. Additionally, the standard synchronous PI controllers are unable to handle unbalanced conditions. Alternatively, the control needs to be implemented for both the positive- and negative-sequence components [13, 17].

Therefore, it is important to improve the steady-state performance of stationary PI controllers. In this regard, modified PI controllers have been reported in the literature. Some of these involve a feedforward controller, which is simple in concept, is robust, and has good dynamic performance [18]. It is especially effective for handling disturbances that can be measured. A stationary PI controller with a grid voltage feedforward path was proposed and applied for grid-tied converters [19]. Its control structure is shown in Fig. 2(a). This strategy improved the transient and disturbance-rejection performance; however, the scheme suffers from voltage background harmonics and stability problems [20].

A combined feedforward–feedback controller, as shown in Fig. 2(b), was proposed in [4] to improve the overall performance of the whole control system. The control strategy described in Fig. 2(b) has been used in other fields [21–24]. However, it has drawn little attention in power electronic converter control. In this paper, a modified PI controller with a current feedforward path is proposed for a three-phase direct MC.

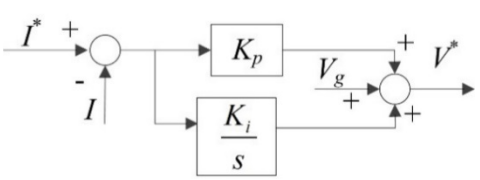

a

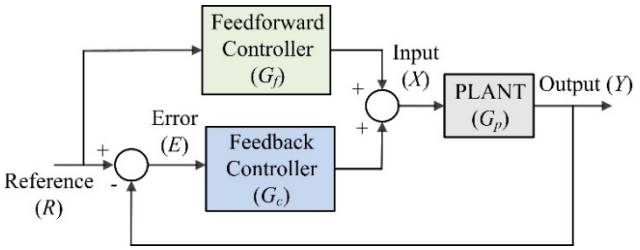

b

Fig. 2. (a) PI controller with a voltage feedforward path. (b) Combined feedforward–feedback controller.

Another potential solution for improving the steady-state tracking performance is the proportional-resonant (PR) controller. The PR controller is a good alternative to conventional PI controllers because it exhibits excellent steady-state performance and can provide specific-order harmonic compensation with reasonable computational burden [5, 25, 26]. It is difficult to achieve harmonic compensation with standard PI controllers. The PR controller has been investigated for converters, and good performance has been reported [27–30]. However, the PR controller and selective-harmonic compensation remain underexplored for the three-phase direct MC. In previous studies, only resonant controllers have been investigated for four-leg MCs, to regulate the output voltage [31]. In this paper, the PR controller is investigated for a three-phase direct MC to control the output currents, and its performance is compared with that of the modified PI controller.

The contributions of this paper are summarized as follows. (a) A modified PI controller with current feedforward in the natural *abc* frame is proposed and tested on an MC. The current feedforward provides extra flexibility for reducing the steady-state error. When the coefficient of current feedforward is equal to the load resistance ($K = R$), the steady-state error is effectively reduced, even with the regulation of the sinusoidal variables. To the knowledge of the authors, this has not been reported in the literature. Unlike the traditional PI controller, the proposed controller does not require frame transformations, because it can be implemented in the natural *abc* frame. Additionally, the modified PI controller can handle unbalanced conditions. (b) The PR controller and selective-harmonic compensation are investigated for the three-phase direct MC to regulate the output currents. The selective harmonics are compensated effectively. The authors believe that the PR controller has not previously been investigated for a three-phase direct MC (shown in Fig. 1). (c) Simulation and experiment comparisons are performed to evaluate and compare the modified PI and PR controllers. It is concluded that the

proposed PI controller is easier to implement and has less steady-state error; whereas, the PR controller is more effective for reducing distortions. The proposed controllers can be applied to not only MCs but also other power electronic converters.

II. PI Controller with Current Feedforward

The proposed combined feedforward–feedback controller is shown in Fig. 2(b), where the current reference is fed forward. The transfer function $E(s)/R(s)$ is given by

$$\frac{E(s)}{R(s)}=\frac{1-G_f(s)G_p(s)}{1+G_c(s)G_p(s)}, \tag{1}$$

where G_c is the PI controller, G_f is the feedforward controller (proportional controller), and G_p is the known resistive–inductive load plant. They are given as follows:

$$G_c(s)=\frac{K_p s+K_i}{s}, \qquad G_f(s)=K, \qquad G_p(s)=\frac{1}{R+Ls}.$$

This is a two-degree-of-freedom control system in which the closed-loop characteristics and the feedback characteristics can be regulated independently to improve the overall performance of the whole system [32]. By rearranging (1), the error in the frequency domain is obtained as

$$E(s)=\frac{1-G_f(s)G_p(s)}{1+G_c(s)G_p(s)}\cdot R(s). \tag{2}$$

The reference R in the natural frame is usually a sinusoidal function $R(t) = I_r\sin(\omega_c t)$, and its frequency-domain expression (Laplace transform) is

$$R(s)=I_r\frac{\omega_c}{s^2+\omega_c^2}, \tag{3}$$

where I_r is the reference amplitude, and $\omega_c = 2\pi f$ is the reference angular frequency. Substituting (3) into (2) yields

$$E(s)=\frac{Ls^2+(R-K)s}{Ls^2+(K_p+R)s+K_i}\cdot I_r\frac{\omega_c}{s^2+\omega_c^2}. \tag{4}$$

To derive the amplitude and phase responses of the error E(s), s is replaced with $j\omega$. Thus, the amplitude and phase angle are obtained as

$$\left|E(j\omega)\right|=\sqrt{\frac{\omega^2L^2+(R-K)^2}{(K_i-\omega^2L)^2+(K_p+R)^2\omega^2}}\cdot\frac{I_r\omega\omega_c}{-\omega^2+\omega_c^2} \tag{5}$$

$$\angle E(j\omega)=\begin{cases}\tan^{-1}\dfrac{(R-K)}{-L\omega}-\tan^{-1}\dfrac{(K_p+R)\omega}{K_i-L\omega^2}, & \omega<\omega_c\\ \tan^{-1}\dfrac{(R-K)}{-L\omega}-\tan^{-1}\dfrac{(K_p+R)\omega}{K_i-L\omega^2}+\pi, & \omega>\omega_c\end{cases}. \tag{6}$$

According to (5) and (6), the error amplitude is minimized when $K = R$ and the other parameters are fixed. The introduction of the feedforward controller offers extra flexibility for tuning the steady-state error performance. The amplitude and phase responses for different values of K are shown in Fig. 3(a). Here, the following parameters are used: $K_p = 10$, $K_i = 1$, $R = 20\ \Omega$, $L = 15$ mH, and $\omega_c = 120\pi$ rad/s. As shown in the figure, the amplitude response for $K = R$ is distinct from the others, and this setting yields the minimum amplitude response for the whole frequency domain. This indicates that an appropriate selection of K can reduce the steady-state error. Fig. 3(b) shows the proposed PI controller with current feedforward for controlling MC output currents. The controller generates the voltage references that are utilized in the SVM to control the MC.

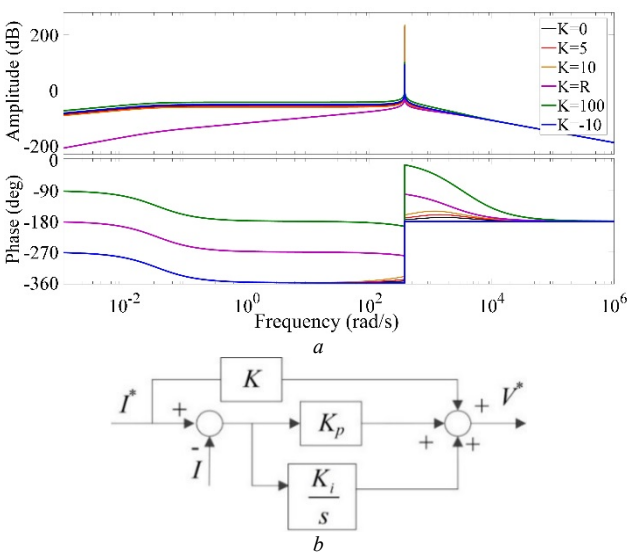

Fig. 3. (a) Bode diagram of $E(j\omega)$ for different values of K. (b) Proposed PI current controller with current feedforward.

Similarly, when the load is resistive–capacitive, i.e.,

$$G_p(s)=\frac{1}{R+1/SC}, \tag{7}$$

the amplitude and angle of the error are

$$\left|E(j\omega)\right|=\sqrt{\frac{1+(R-K)^2C^2\omega^2}{(1+K_iC)^2+(K_p+R)^2C^2\omega^2}}\cdot\frac{I_r\omega_c}{-\omega^2+\omega_c^2} \tag{8}$$

$$\angle E(j\omega)=\begin{cases}\tan^{-1}(R-K)C\omega-\tan^{-1}\dfrac{(K_p+R)C\omega}{1+K_iC}, & \omega<\omega_c\\ \tan^{-1}(R-K)C\omega-\tan^{-1}\dfrac{(K_p+R)C\omega}{1+K_iC}+\pi, & \omega>\omega_c\end{cases}. \tag{9}$$

As indicated by (8) and (9), we can obtain the same conclusion as that for the *RL* load.

Compared with the traditional PI controller, the proposed method has reduced steady-state error with the regulation of the sinusoidal variables. This is achieved by introducing a current feedforward path in the controller. This current feedforward path provides extra flexibility for reducing the steady-state error. The proposed method does not require frame transformations, because it can be implemented in the natural *abc* (stationary) frame, which reduces the implementation demands. Although the proposed controller requires three controllers, it can easily handle unbalanced conditions because it can be individually implemented for each phase. Thus, the computational burden of the proposed controller is reduced compared with the *dq*-frame based controller.

In this study, only the known resistive–inductive and resistive–capacitive loads are considered. When the load is more complex or unknown, load-parameter identification and modeling techniques such as the hybrid learning algorithm [33], Kalman filter-based estimation [34], and least-squares methods [35, 36] can be utilized. The feedforward controller can be designed depending on the specific application to achieve the desired results. This topic remains open, and future research is required.

III. PR Controller with Harmonic Compensation

The PR controller can provide an infinite gain at the target frequencies to eliminate the steady-state error at these frequencies and to compensate for selective harmonic contents by cascading multiple PR controllers [20, 37].

A. PR Controller

In principle, the PR controller can be derived by transforming a desired DC compensation network into an equivalent AC compensation network [38]. This is conceptually similar to transforming a synchronous reference frame-based PI controller into a stationary frame-based controller [20]. The PR controller is expressed as

$$G_{PR}(s)=K_P+\frac{2K_Rs}{s^2+\omega^2}, \tag{10}$$

where K_P and K_R are the proportional and resonant gains, respectively. This controller can provide an infinite gain at the frequency ω and cause no phase shift at other frequencies. However, it is not practical to implement an ideal PR controller, because of the infinite quality factor [25]. Hence, the nonideal PR controller is usually adopted, which is expressed as follows:

$$G_{PR}(s)=K_P+\frac{2K_R\omega_cs}{s^2+2\omega_cs+\omega^2}. \tag{11}$$

Here $\omega_c << \omega$ is the cutoff frequency, which affects the bandwidth around the target resonance frequencies. The nonideal PR controller has a larger bandwidth around the target frequencies, which leads to less sensitivity and more robustness. Thus, the nonideal PR controller is more robust to frequency variations around the target frequencies.

B. PR Controller with Harmonic Compensation

To compensate for harmonics, several PR controllers with different resonant frequencies are cascaded. The ideal PR controller with a harmonic compensator is expressed as

$$G_{PR}(s)=K_P+\sum_{n=1,3,5,7}\frac{2K_{Rn}s}{s^2+(n\omega)^2}, \tag{12}$$

and the nonideal PR controller with a harmonic compensator is expressed as

$$G_{PR}(s)=K_P+\sum_{n=1,3,5,7}\frac{2K_{Rn}\omega_cs}{s^2+2\omega_cs+(n\omega)^2}, \tag{13}$$

where n is the harmonic order, and K_{Rn} is the individual resonant gain for the n^{th}-order harmonic. Diagrams of the ideal and nonideal PR controllers with the harmonic compensator are shown in Figs. 4(a) and (b), respectively. Their frequency responses are shown in the Bode plots of Figs. 4(c) and (d), respectively. The gains at the resonant frequencies can be tuned as required. In Figs. 4(c) and (d), $K_P = K_{Rn} = 1$ is used for simplicity.

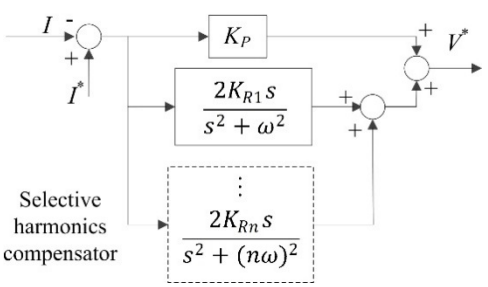

a

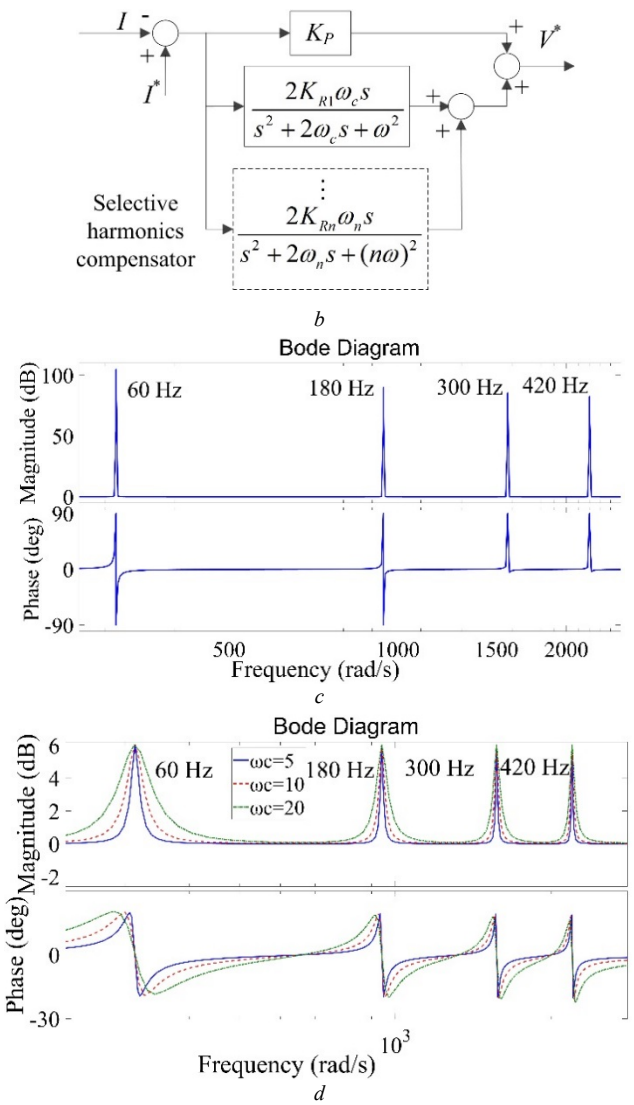

Fig. 4. Diagrams of (a) ideal and (b) nonideal PR controllers with selective-harmonic compensation. Bode diagrams of (c) ideal PR controller and (d) nonideal PR controllers with harmonic compensation (K_P = 1, K_{Rn} = 1, ω = 120π rad/s).

The target resonant frequencies in the harmonic compensator can be designed for specific applications. The 3rd, 5th, and 7th harmonics are usually considered, because they are regarded as the most prominent harmonics in a typical current spectrum [37].

As shown in Figs. 4(c) and (d), the PR controller and harmonic compensator can provide large gains at the target frequencies. Compared with the ideal PR controller, the nonideal PR controller has a larger bandwidth around the target frequencies, which results in better robustness to frequency variations.

The error of the MC output current passes through the PR controller, providing the voltage references. These references are then delivered to the SVM modulation stage to generate the gating pulses for the MC. The MC input current can also be controlled by the proposed scheme, and the input power factor can be regulated to unity. The PR-controller parameters should be tuned appropriately to obtain the desired performance, which can be done via a method similar to that for the PI controller.

IV. MC AND SVM

A. MC Basics

As shown in Fig. 1, a three-phase direct MC consists of nine bidirectional switches. These switches form a 3 × 3 switch matrix, as follows:

$$\begin{bmatrix} v_a \\ v_b \\ v_c \end{bmatrix} = \begin{bmatrix} S_{Aa} & S_{Ba} & S_{Ca} \\ S_{Ab} & S_{Bb} & S_{Cb} \\ S_{Ac} & S_{Bc} & S_{Cc} \end{bmatrix} \begin{bmatrix} v_A \\ v_B \\ v_C \end{bmatrix} = S \begin{bmatrix} v_A \\ v_B \\ v_C \end{bmatrix} \tag{14}$$

$$\begin{bmatrix} i_A \\ i_B \\ i_C \end{bmatrix} = \begin{bmatrix} S_{Aa} & S_{Ab} & S_{Ac} \\ S_{Ba} & S_{Bb} & S_{Bc} \\ S_{Ca} & S_{Cb} & S_{Cc} \end{bmatrix} \begin{bmatrix} i_a \\ i_b \\ i_c \end{bmatrix} = S^T \begin{bmatrix} i_a \\ i_b \\ i_c \end{bmatrix} \tag{15}$$

$$\sum_{X=A,B,C} S_{Xx} = 1, \ (x = a,b,c) \ , \tag{16}$$

where S (transpose S^T) is the switch matrix. The elements S_{Xx} in the switch matrix can be assigned a value of 1 (for the "on" state) or 0 (for the "off" state).

The constraints (16) are applied to exclude switch states that short-circuit the inputs (usually voltage sources) or open-circuit the outputs (usually inductive loads). Otherwise, overcurrent or overvoltage is generated. A total of 27 switch states are allowable in the matrix, which are represented by 27 control actions (finite control set).

B. SVM of MC

A synchronous frame-based PI controller using SVM was proposed in [39] and [40] for an MC to control the power flow in a transmission system. However, the issues associated with synchronous PI controllers persisted. In this study, a modulation stage based on the indirect SVM is adopted to generate the firing pulses for the proposed controllers. There are two methods for implementing the indirect SVM in the controllers: direct and indirect [5].

In the direct method, the output voltage and input current references are directly used in the SVM control to generate gating pulses for the semiconductor switches in the MC [40]. The output voltage reference is generated by the current controller, which forms a current loop. The MC input

current references are specified according to the system requirements.

In the indirect method, the SVM is divided into virtual inversion and rectification modulation stages, as shown in Fig. 5. In the virtual inversion modulation stage, the designed current controller and SVM (for the inverter only) are used to generate gating pulses for the semiconductor switches in the virtual inverter. SVM (for the rectifier only) is used in the virtual rectification modulation stage to generate gating pulses for the semiconductor switches in the virtual rectifier. Then, the two virtual modulation stages are combined to control the MC [39]. In this study, the indirect approach is used.

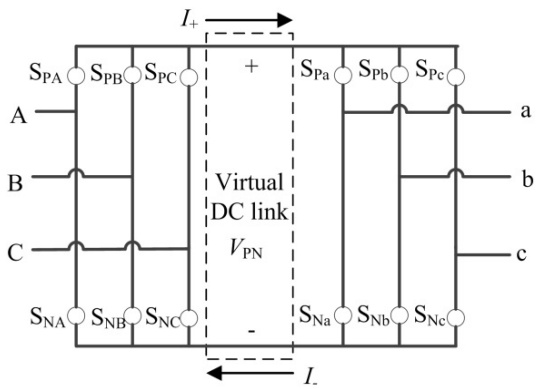

Fig. 5. Indirect SVM with a virtual DC link.

In the indirect SVM control, the virtual DC link—shown in Fig. 5—is used to connect the virtual voltage source rectifier and the virtual voltage source inverter. The virtual DC link does not actually exist in the MC. It is only used to explain the modulation technique. By applying SVM to the different stages and combining them, the overall indirect SVM for the MC can be derived. As a result, the time durations (duty cycles) of the switch states for the overall combined modulation stage are derived:

$$t_{\gamma\alpha} = m\sin\left(\frac{\pi}{3}-\theta_R\right)\sin\left(\frac{\pi}{3}-\theta_I\right) \tag{17}$$

$$t_{\delta\alpha} = m\sin\left(\theta_R\right)\sin\left(\frac{\pi}{3}-\theta_I\right) \tag{18}$$

$$t_{\gamma\beta} = m\sin\left(\frac{\pi}{3}-\theta_R\right)\sin\left(\theta_I\right) \tag{19}$$

$$t_{\delta\beta} = m\sin\left(\theta_R\right)\sin\left(\theta_I\right) \tag{20}$$

$$t_0 = T_s - \left(t_{\gamma\alpha} + t_{\delta\alpha} + t_{\gamma\beta} + t_{\delta\beta}\right), \tag{21}$$

where $t_{\gamma\alpha}$, $t_{\delta\alpha}$, $t_{\gamma\beta}$, $t_{\delta\beta}$, and t_0 are the time durations for the active (1) and inactive (0) switch states, and T_s is the sampling interval. θ_R (θ_I) (where $0 \le \theta_R\,(\theta_I) \le \pi/3$) is the angle between the desired space vector I_{RS} (V_{IS}) and the right-hand-side adjacent vector $I_{R\gamma}$ ($V_{I\alpha}$). $m = m_i \times m_v$ is the modulation index. Additional details on obtaining the time durations are presented in [4, 40, 41].

TABLE I Duty-cycle distribution for the symmetric switching sequence.

	$t_{\gamma\alpha}/2$	$t_{\delta\alpha}/2$	$t_{\delta\beta}/2$	$t_{\gamma\beta}/2$	t_0	$t_{\gamma\beta}/2$	$t_{\delta\beta}/2$	$t_{\delta\alpha}/2$	$t_{\gamma\alpha}/2$
S_{Aa}	1	1	1	1	0	1	1	1	1
S_{Ba}	0	0	0	0	0	0	0	0	0
S_{Ca}	0	0	0	0	1	0	0	0	0
S_{Ab}	0	1	1	0	0	0	1	1	0
S_{Bb}	1	0	0	0	0	0	0	0	1
S_{Cb}	0	0	0	1	1	1	0	0	0
S_{Ac}	0	0	0	0	0	0	0	0	0
S_{Bc}	1	1	0	0	0	0	0	1	1
S_{Cc}	0	0	1	1	1	1	1	0	0

To reduce the switching transitions between the switch states, a symmetric switching sequence is employed in each sampling interval T_s. This is achieved using the location information (k_i and k_v) of the input current and output voltage space vectors. An example is presented in Table I for $k_i = k_v = 1$. In this table, a value of "1" indicates that the corresponding switch is turned on for the designated time segments, and a value of "0" indicates that the switch is turned off. As indicated by this table, in one sampling period, only one switching transition is required between each state. A switching lookup table can be obtained in a similar manner. Accordingly, an enhanced pulse-width modulator (ePWM) can be implemented by assigning the compare registers appropriate values.

V. Simulation Tests

According to the foregoing analyses of the proposed controllers and SVM, the proposed PI and PR controllers for the SVM-modulated MC can be designed, as shown in Figs. 6(a) and (b), respectively. These controller structures are simple, and no frame transformations are required, because they are implemented in the natural *abc* system. To control the input power factor, a phase-locked loop is used to detect the location of the input voltages. The parameters of the simulation system are presented in Table II. The output frequency is 60 Hz. In the tested RL load, the filtering effect of the inductor is limited; thus, the current waveform is poor,

as indicated by the following results. Nonetheless, these comparative results verify the effectiveness of the proposed controller. The current waveform can be significantly improved by increasing the inductance. For simple and explicit figure captions, the tested controllers are abbreviated as follows: open-loop SVM (SVM), PI-based SVM (PI-SVM), PI with current feedforward-based SVM (PICF-SVM), PR-based SVM (PR-SVM), and PR with harmonic compensation-based SVM (PRHC-SVM).

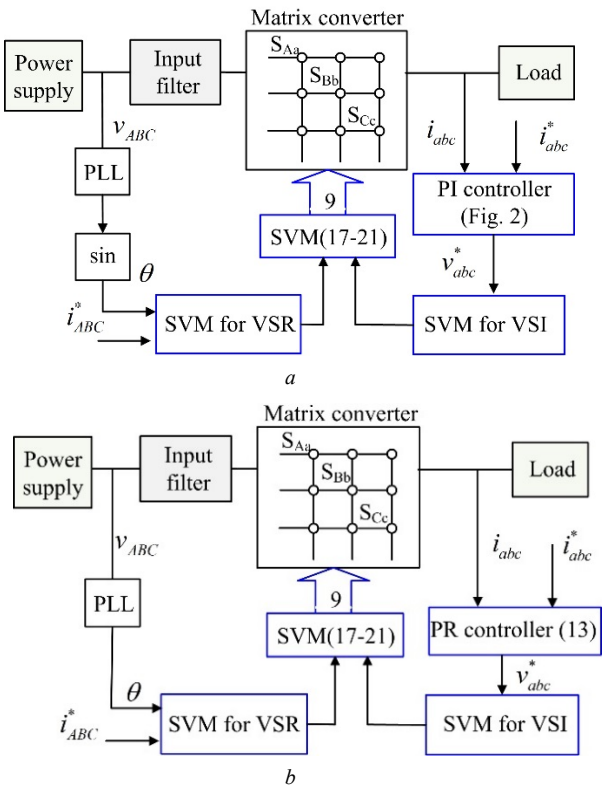

Fig. 6. (a) Proposed PI controller for the MC and (b) PR controller for the MC.

TABLE II Simulation parameters.

V_i [V]	f_i [Hz]	L_A [mH]	r_A [Ω]	C_{AB} [μF]	L [mH]	R [Ω]	T_s [μs]
100	50	4.8	30	10	14	20.3	100

Comparative simulation results for the PI controller with current feedforward are presented in Fig. 7. The parameters used in the PI controller are K_p = 200 and K_i = 10. The simulation results for the traditional PI controller (in the *abc* frame) are shown in Figs. 7(a) and (c). A significant steady-state error appears in the waveform. The fundamental reference current amplitude is 3.6 A, while the regulated fundamental current amplitude only reaches 3.22 A with total harmonic distortion (THD) of 10.27%. In contrast, the steady-state error performance is significantly improved for the proposed PI controller with current feedforward ($K = R$ = 20.3, while K_p and K_i are the same as before), as shown in Figs. 7(b) and (d). The steady-state current amplitude reaches 3.53 A, and the THD is reduced to 7.80%. The MC input voltage and current of phase A are presented in Fig. 7(e). As shown, the MC input current is almost in phase with the input voltage. A small phase shift is caused by the input filters, because the input current is controlled in the open-loop approach.

The dynamic response of the proposed controller to the current-amplitude change from 2.8 to 3.6 A at 0.05 s is shown in Fig. 7(f). This result shows the fast transient response of the proposed controller. Additionally, the modulation index of the MC influences the controller performance. This is observed in Fig. 7(f), where different current amplitudes correspond to different modulation indices.

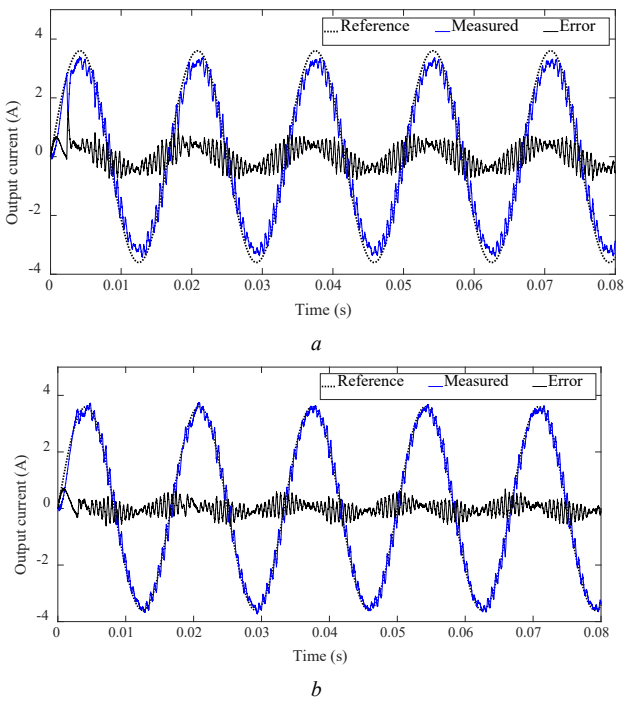

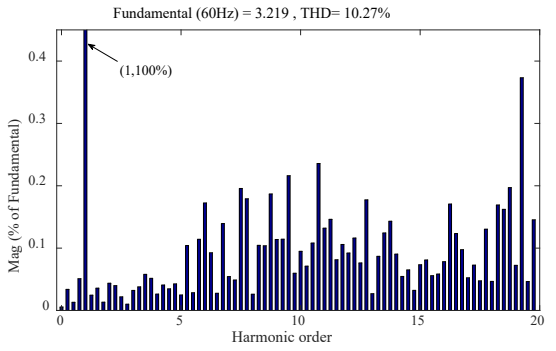

c

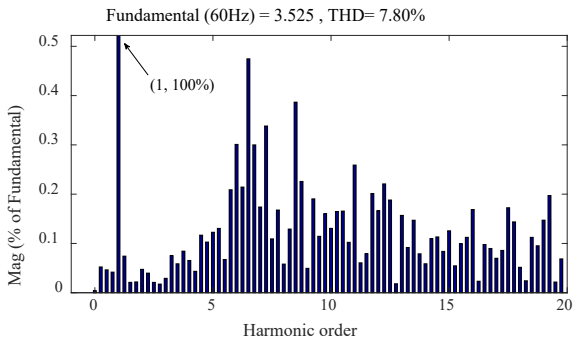

d

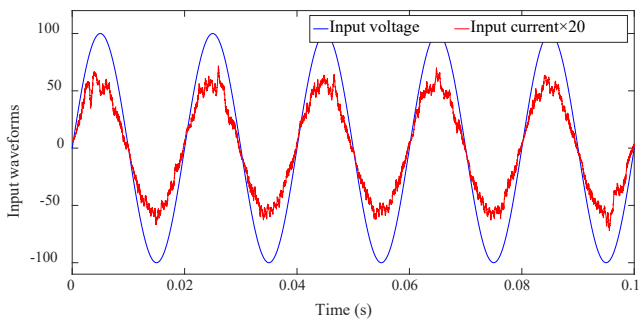

e

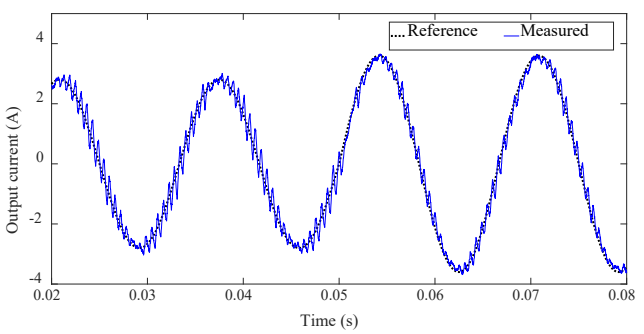

f

Fig. 7. Simulation results: (a) PI-SVM steady-state output current, (b) PICF-SVM steady-state output current, (c) PI-SVM FFT analysis of the current, (d) PICF-SVM FFT analysis of the current, (e) MC input phase current and voltage (PICF-SVM), and (f) transient performance of the PICF-SVM controller.

The test results obtained under unbalanced conditions and input variations are shown in Fig. 8. For unbalanced conditions, the resistance of the output phase *b* is reduced to half of that of the other two output phases, and the voltage amplitude of input phase *A* is reduced by 20% (as shown in Fig. 8(a)). As shown in Fig. 8(b), the output currents can be regulated effectively under unbalanced conditions. For the input variation, the sudden changes in both the voltage (by -15 V) and phase (by 30°) of input phase *A* are simulated, as shown in Fig. 8(c). As shown in Fig. 8(d), the output current is only slightly affected, and the results are acceptable. If the unbalanced condition or input variation deteriorates, the results become worse than those for most of the other control methods.

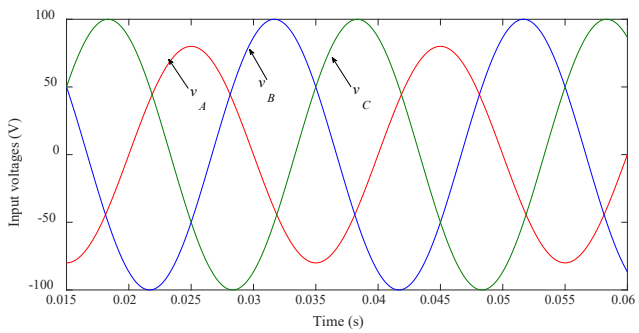

a

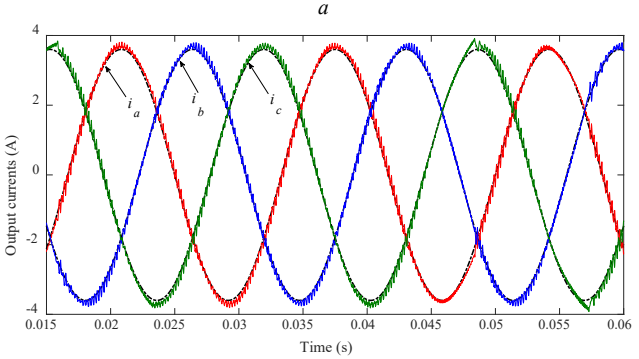

b

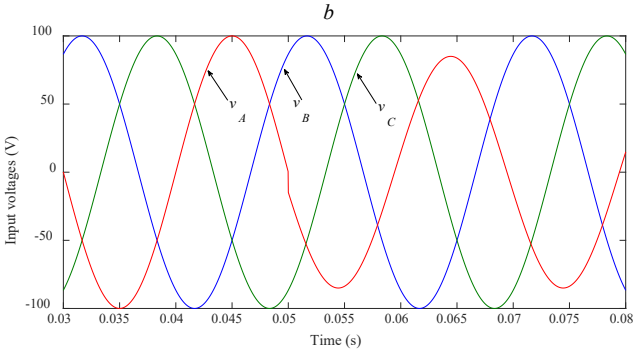

c

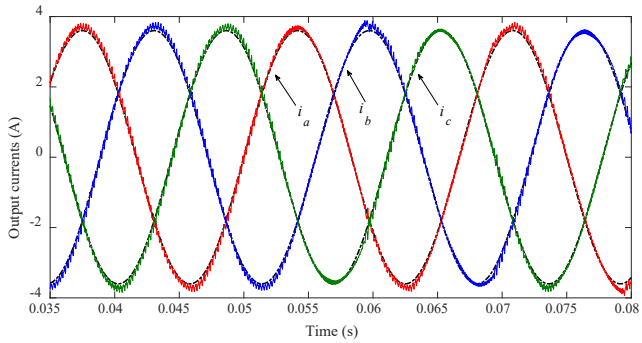

d

Fig. 8. Simulation results under unbalanced conditions and input variation: (a) unbalanced input voltages, (b) regulated output currents, (c) input voltages with a sudden change, and (d) regulated output currents.

The simulation results for the PR controller are shown in Fig. 9. The controller parameters are as follows (unless otherwise specified): $K_P = 350$, $K_{RI} = 600$, K_{Rn} (n =1, 2, 3, 4, 5, 6, 7) = 0, $\omega = 120\pi$ rad/s, and $\omega_c = 2\pi$ rad/s.

Fig. 9(a) shows the steady-state current of the PRHC-SVM controller. The simulated current for PR-SVM is not shown, because it is very similar to that for PRHC-SVM. As shown in Fig. 9(a), the steady-state tracking error is not significant. Figs. 9(b) and (c) compare the fast Fourier transform (FFT) analysis results for PR-SVM and PRHC-SVM. As shown in Fig. 9(b), the 4th, 6th, and 7th harmonics are significant for PR-SVM; therefore, these harmonics are compensated for in PRHC-SVM. The FFT analysis results for PRHC-SCM are shown in Fig. 9(c). The specific harmonics (6th and 7th) are suppressed appreciably, and the controller is effective. The gain of each compensator determines the corresponding control effectiveness. The reduction of the specific harmonics may increase other harmonics; therefore, a compromise must be achieved when designing the controller. Fig. 9(c) presents a compromised result, which is the reason for the slight increase in the 4th-order harmonic distortion.

The selective-harmonic compensator does not necessarily improve the overall THD performance. In fact, it affects the harmonic spectrum, because increasing the gain for other order harmonics changes the relative gain of each harmonic. The THD of the MC output current is influenced by the modulation index (voltage transfer ratio). With the PR-SVM and PRHC-SVM control schemes, the input power factor can be regulated and can reach unity.

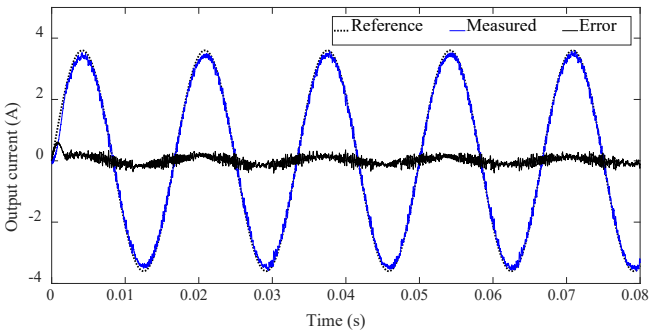

a

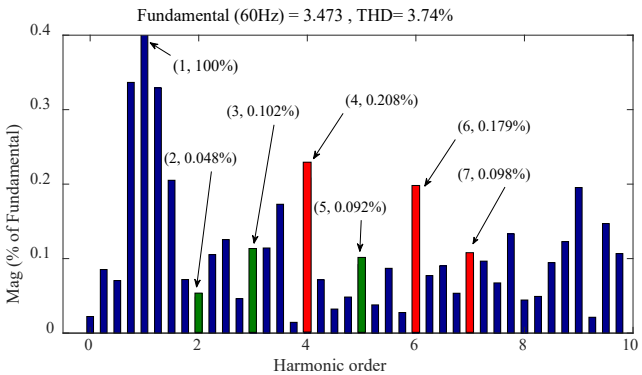

b

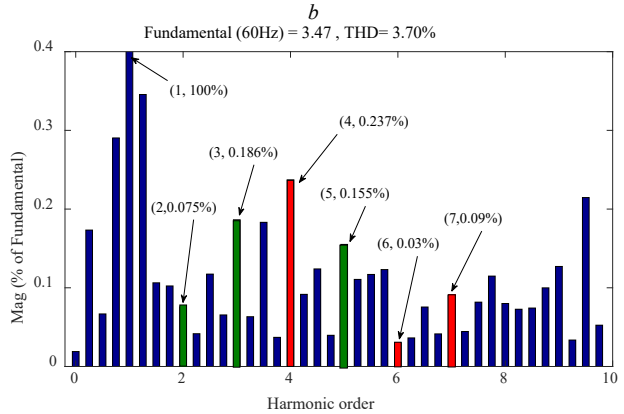

c

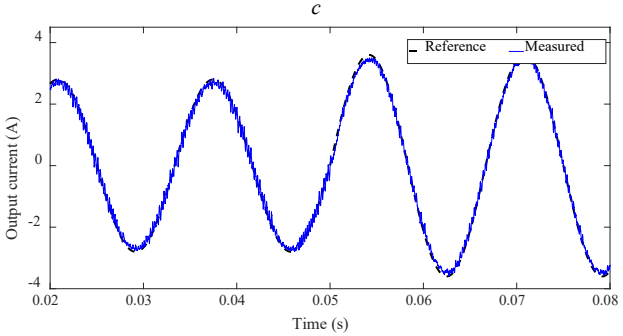

d

Fig. 9. (a) Steady-state performance of the PRHC-SVM-controlled output current, (b) FFT analysis of the PR-SVM-controlled output current, (c) FFT analysis of the PRHC-SVM-controlled output current, and (d) dynamic response of PRHC-SVM to a step reference (for PRHC-SVM: $K_{R4} = K_{R6} = 500$, $K_{R7} = 300$).

In Fig. 9(d), the dynamic response of the proposed controller to a step change in the reference current from 2.8 to 3.6 A is evaluated. The controller exhibits a good dynamic response, and the prescribed reference is tracked effectively.

The foregoing steady-state simulation results are summarized in Table III. The modified PI controller exhibits an improved steady-state performance, particularly with regard to the error, whereas the PR controller has better performance with regard to the THD.

TABLE III Simulation results for PI-SVM, PICF-SVM, PR-SVM, and PRHC-SCM.

Method	PI-SVM	PICF-SVM	PR-SVM	PRHC-SVM
Error	0.381	0.075	0.127	0.13
THD	10.27%	7.8%	3.74%	3.7%

VI. Experimental Validation

To verify the proposed strategies, an MC was constructed and used for an experiment. The experimental setup is shown in Fig. 10. Bidirectional switches (insulated-gate bipolar transistors, IGBTs) were arranged in the common collector configuration. As a result, only six independent driver power supplies were needed to drive 18 IGBTs. The control card was a TI TMS320F28377D series digital signal processor (DSP) board. The real-time control was implemented in MATLAB/Simulink with C2000 hardware support packages. A serial communications interface was used for the communication between the host computer and DSP card. Analog-to-digital conversion (ADC) and peripheral circuits were employed to process the signals from the voltage and current sensors. The carrier waveform used in the modulation stage was generated from the ePWM blocks, which facilitated the implementation of the symmetric switching sequence.

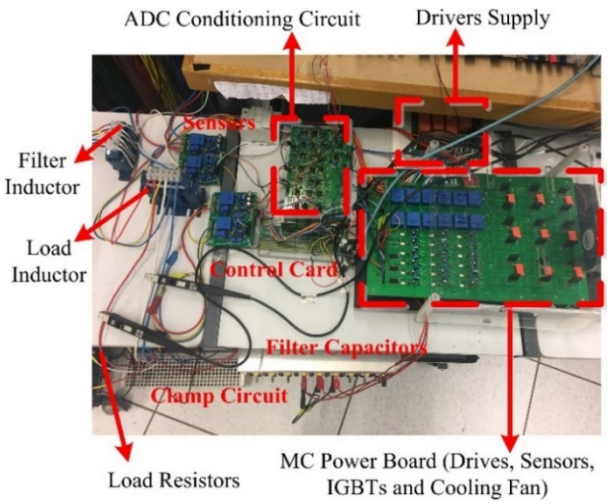

Fig. 10. MC prototype.

In the experimental tests, the parameters of the controllers were set to the same values used in the simulation, unless otherwise specified. The steady-state experimental results are presented in Figs. 11–13 and Tables IV and V.

The experimental waveforms for SVM are presented in Figs. 11(a) and (b). As shown, the SVM-controlled MC generated sinusoidal waveforms. However, the open-loop SVM was ineffective for controlling the output currents when the load was unknown.

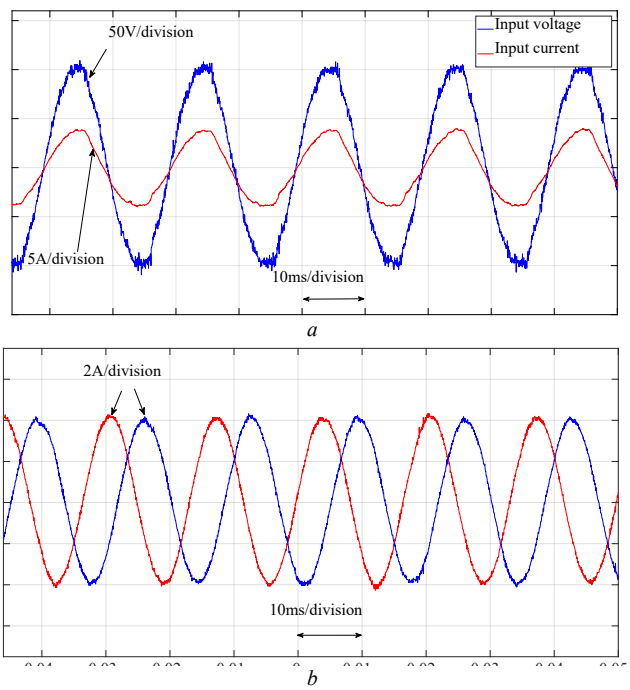

Fig. 11. (a) Input voltage and current, (b) output currents (two phases).

Fig. 12 presents the experimental results for PI-SVM and

PICF-SVM. The steady-state tracking error of PI-SVM was significant, as shown in Fig. 12(a). However, for the proposed PICF-SVM controller, when the reference was 3.6 A, the fundamental current amplitude was improved from 3.34 to 3.56 A, and the THD was reduced from 12.05% to 9.01%. These results are shown in Figs. 12(c) and (d). The PI-SVM and PICF-SVM controllers exhibited very similar performance with regard to the input current regulation, as shown in Figs. 12(e) and (f). The input power factor was regulated to be close to unity (1).

Compared with the open-loop SVM, the closed-loop SVM exhibited more severe distortion in the output current. This is because the modulation index changed continuously in the closed-loop SVM. In previous studies, the effect of the modulation index on the current-regulation performance was investigated. A general conclusion is that a lower modulation index yields greater current distortion [42].

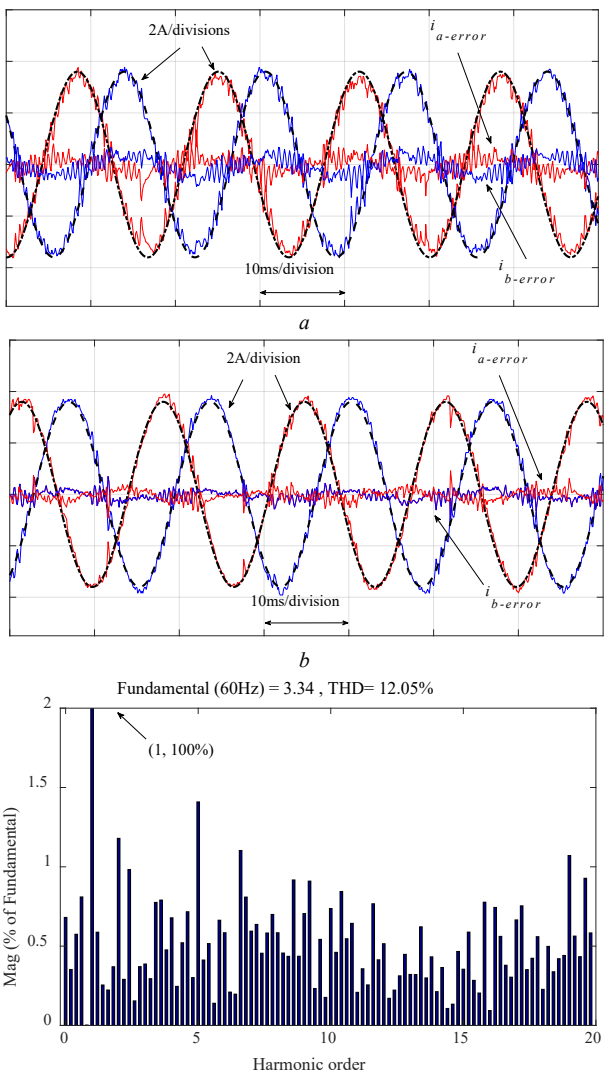

Fig. 12. Experimental results of PI-SVM and PICF-SVM: (a) PI-SVM output currents, (b) PICF-SVM output currents, (c) PI-SVM output current FFT analysis, (d) PICF-SVM output current FFT analysis, (e) PI-SVM input voltage and current, and (f) PICF-SVM input voltage and current.

The comparative experimental results for PR-SVM and PRHC-SVM are illustrated in Fig. 13 and Tables IV and V. The performance of the input current regulation was similar to that for PICF-SVM; therefore, these results are not presented. The experimental waveforms of the PR-SVM-controlled output currents and FFT analysis results are presented in Figs. 13(a) and (c), respectively. Here, the 3rd, 4.2th, and 6.8th harmonics are more significant; thus, the 3rd, 4th, and 6th harmonics are compensated for in the PRHC-SVM scheme.

Figs. 13(b) and (d) show the PRHC-SVM-controlled

output currents and FFT analysis results. Table IV compares the low-order harmonics between PR-SVM and PRHC-SVM. These results indicate that the PRHC-SVM compensated the selective-order harmonics effectively.

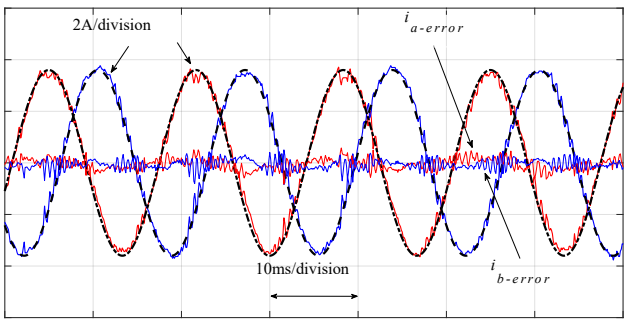

a

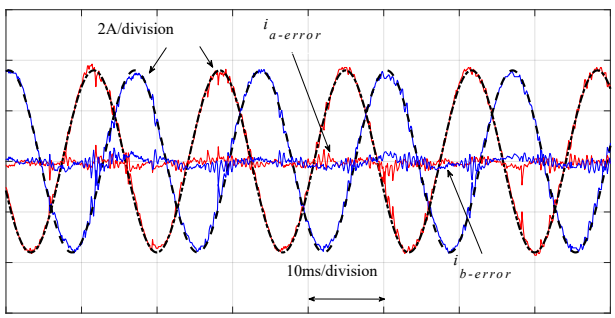

b

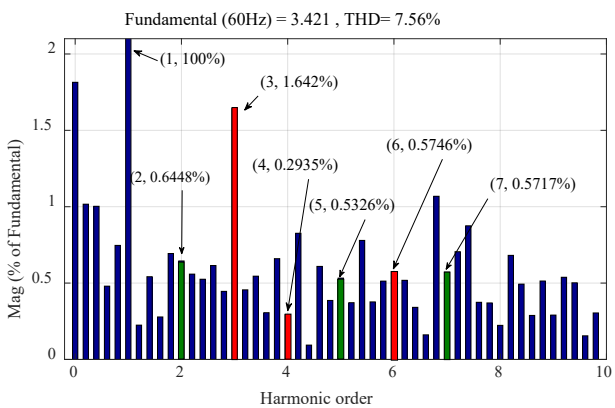

c

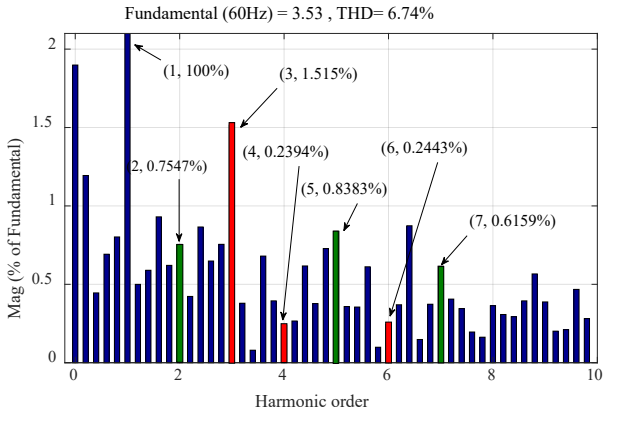

d

Fig. 13. Experimental results: (a) PR-SVM output currents, (b) PRHC-SVM output currents, (c) PR-SVM output current FFT analysis, and (d) PRHC-SVM output current FFT analysis (for PRHC-SVM: K_{R3} = 500, K_{R4} = 200, K_{R6} = 300).

Table V presents the steady-state experimental results. These results are consistent with the simulation results in Table III. Compared with the PR controller, the modified PI controller was more effective for reducing the steady-state errors. However, the PR controller had less THD. The controllers were tested on an MC in this study, but they can easily be extended to other converters.

TABLE IV Comparison of the low-order harmonics between PR-SVM and PRHC-SVM.

Harmonic	2nd	3rd	4th	5th	6th	7th
PR-SVM	0.6448	1.642	0.2935	0.5326	0.5764	0.5717
PRHC-SVM	0.7547	1.515	0.2394	0.8383	0.2443	0.6159

TABLE V Experimental comparison of PI-SVM, PICF-SVM, PR-SVM, and PRHC-SCM.

Method	PI-SVM	PICF-SVM	PR-SVM	PRHC-SVM
Error	0.26	0.04	0.179	0.07
THD	12.05%	9.01%	7.56%	6.74%

VII. Conclusions

To improve the steady-state tracking performance, a combined feedforward–feedback PI controller was proposed, and a PR controller was investigated. These controllers were tested on an MC. Both controllers exhibited reduced steady-state tracking error and THD. First, a modified PI controller with current feedforward was proposed. The

introduction of the feedforward control provided extra freedom for reducing the steady-state error. Analysis indicated that the minimum tracking error can be achieved when the coefficient of the current feedforward is equal to the load resistance ($K = R$). Then, a PR controller with the capability of compensating selective-order harmonics was investigated for the MC. Both of the proposed controllers are simple and easy to implement. They do not require reference-frame transformations, because they can be straightforwardly implemented in the natural *abc* frame. Consequently, the implementation effort is reduced. The ability to handle unbalanced conditions is an advantage of both the modified PI and PR controllers. A constant switching frequency is achieved because of the SVM modulation stage. Comparative analysis revealed that the proposed PI controller is easier to implement and has less steady-state error, while the PR controller is more effective for reducing distortions.

Simulation and experimental results corroborate the effectiveness of the proposed controllers. These controller schemes can be readily extended to other power electronic converters and used in many applications, such as grid synchronization and microgrids.

REFERENCES

[1] P. Wheeler, J. Rodriguez, J. Clare, L. Empringham, A. Weinstein, "Matrix converters: a technology review," *IEEE Trans Ind Electron*, vol. 49, no. 2, pp. 276-288, 2002.

[2] J. Zhang, L. Li, and D. G. Dorrell, "Control and applications of direct matrix converters: A review." Chinese J. Electrical Engineering, vol. 4, no. 2, pp. 18-27, 2018.

[3] H. Altun, S. Sünter, "Matrix converter induction motor drive: modeling, simulation and control," *Electrical Engineering*, vol. 86, no. 1, pp. 25-33, 2003.

[4] J. Zhang, L. Li, D. G. Dorrell, Y. Guo, "A PI Controller with Current Feedforward to Improve the Steady-State Error Performance for the Current Controlled Direct Matrix Converter," *20th Int. Conf. Electrical Machines Systems*, Sydney, Australia, 2017

[5] J. Zhang, L. Li, D. G. Dorrell, Y. Guo, "SVM based Proportional Resonant Current Controller with Selective Harmonics Compensation for Matrix Converter Systems," *20th Int. Conf. Electrical Machines Systems*, Sydney, Australia, 2017.

[6] H. Altun, S. Sünter, "Modeling, simulation and control of wind turbine driven doubly-fed induction generator with matrix converter on the rotor side," *Electrical Engineering*, vol. 95, no. 2, pp. 157-170, 2013.

[7] J. Zhang, H. Yang, T. Wang, L. Li, L., D. G. Dorrell, D. D. C. Lu, "Field-oriented control based on hysteresis band current controller for a permanent magnet synchronous motor driven by a direct matrix converter," *IET Power Electronics*, vol. 11, no. 7, pp. 1277-1285, 2018.

[8] Yaskawa, "Low Harmonics Regenerative Matrix Converter U1000," [online]. http://www.pillar.com.mx/Varios/CATALOGO%20TECNICO%20U1000.pdf

[9] Yaskawa, AC7 Matrix Drive. [online]. https://www.yaskawa.com/products/drives/industrial-ac-drives/general-purpose-drives/ac7-matrix-drive

[10] M. Munzer, "EconoMac – the First All In One IGBT Module for Matrix Converters," *Drives and Control Conf.*, Section 3, London, 2011.

[11] J. I. Itoh, A. Odaka, I. Sato, "High efficiency power conversion using a matrix converter," *Fuji Electric Review*, vol. 50, no. 3, pp. 94-98, 2014.

[12] E. Yamamoto, J. K. Kang, H. P. Krug, "Development of Matrix Converter for Industrial Applications," *Yaskawa White Paper*, 2007.

[13] J. Rocabert, A. Luna, F. Blaabjerg, P. Rodriguez, "Control of power converters in AC microgrids," *IEEE Trans. Power Electronics*, vol. 27, no. 11, pp. 4734-4749, 2012.

[14] H. H. Choi, E. K. Kim, D. Y. Yu, J. W. Jung, T. H. Kim, "Precise PI speed control of permanent magnet synchronous motor with a simple learning feedforward compensation," *Electrical Engineering*, vol. 99, no. 1, pp. 133-139, 2017.

[15] Y. Han, P. Shen, J. M. Guerrero, "Stationary frame current control evaluations for three-phase grid-connected inverters with PVR-based active damped LCL filters," *Journal of Power Electronics*, vol. 16, no. 1, pp. 297-309, 2016.

[16] X. Yuan, W. Merk, H. Stemmler, J. Allmeling, "Stationary-frame generalized integrators for current control of active power filters with zero steady-state error for current harmonics of concern under unbalanced and distorted operating conditions," *IEEE Trans. Industry Applications*, vol. 38, no. 2, pp. 523-532, 2012.

[17] M. Liserre, R. Teodorescu, F. Blaabjerg, "Multiple harmonics control for three-phase grid converter systems with the use of PI-RES current controller in a rotating frame," *IEEE Trans. Power Electronics*, vol. 21, no. 3, pp. 836-841, 2006.

[18] R. Redl, "Feedforward control of switching regulators," *Analog Circuit Design*, Springer Netherlands, pp. 321-338, 2012.

[19] G. Shen, D. Xu, L. Cao, X. Zhu, "An improved control strategy for grid-connected voltage source inverters with an LCL filter," *IEEE Trans. Power Electronics*, vol. 23, no. 4, pp. 1899-1906, 2008.

[20] R. Teodorescu, F. Blaabjerg, M. Liserre, P. C. Loh, "Proportional-resonant controllers and filters for grid-connected voltage-source converters," *IEE Proceedings-Electric Power Applications*, vol. 153, no. 5, pp. 750-762, 2006.

[21] H. Zhang, J. Wang, "Combined feedback–feedforward tracking control for networked control systems with probabilistic delays," *Journal of the Franklin Institute*, vol. 351, no. 6, pp. 3477-3489, 2014.

[22] J. Elso, M. Gil-Martínez, M. García-Sanz, "Quantitative feedback–feedforward control for model matching and disturbance rejection," *IET Control Theory & Applications*, vol. 7, no. 6, pp. 894-900, 2013.

[23] L. Y. Pao, J. A. Butterworth, D. Y. Abramovitch, "Combined feedforward/feedback control of atomic force microscopes," *In American Control Conference*, *ACC'07*, pp. 3509-3515, 2007.

[24] R. M. Guo, "Modeling and simulation of run-out table cooling control using feedforward-feedback and element tracking system," *IEEE Trans. Industry Applications*, vol. 33, no. 2, pp. 304-311, 1997.

[25] H. Cha, T. Vu, J. Kim, "Design and control of Proportional-Resonant controller based Photovoltaic power conditioning system," *IEEE Energy Conversion Congr. Exposition*, San Jose, California, pp. 2198-2205, 2009.

[26] A. Timbus, M. Liserre, R. Teodorescu, P. Rodriguez, F. Blaabjerg, "Evaluation of current controllers for distributed power generation systems," *IEEE Trans. Power Electronics*, vol. 24, no. 3, pp. 654-664, 2009.

[27] B. Li, W. Yao, L. Hang, L. M. Tolbert, "Robust proportional resonant regulator for grid-connected voltage source inverter (VSI) using direct pole placement design method," *IET Power Electronics*, vol. 5, no. 8, pp. 1367-1373, 2012.

[28] A. Vidal, F. D. Freijedo, A. G. Yepes, J. Malvar, Ó. López, J. Doval-Gandoy, "Transient response evaluation of stationary-frame resonant current controllers for grid-connected applications," *IET Power Electronics*, vol. 7, no. 7, pp. 1714-1724, 2014.

[29] A. R. López, J. D. Mina, G. Calderón, J. Aguayo, J. H. Calleja, "Combined parameters selection of a proportional integral plus resonant

controller for harmonics compensation in a wind energy conversion system," *Electrical Engineering*, 1-10, 2018.

[30] G. Shen, X. Zhu, J. Zhang, D. Xu, "A new feedback method for PR current control of LCL-filter-based grid-connected inverter," *IEEE Trans. Industrial Electronics*, vol. 57, no. 6, pp. 2033-2041, 2010.

[31] R. Cárdenas, C. Juri, R. Peña, P. Wheeler, J. Clare, "The application of resonant controllers to four-leg matrix converters feeding unbalanced or nonlinear loads," *IEEE Trans.Power Electronics*, vol. 27, no. 3, pp. 1120-1129, 2012.

[32] K. Ogata, " PID controllers and modified PID controllers', *Modern Control Engineering*, *fifth edition*, PEARSON, pp. 577-651, 2010.

[33] H. Bai, P. Zhang, V. Ajjarapu, "A novel parameter identification approach via hybrid learning for aggregate load modeling," *IEEE Trans. Power Systems*, vol. 24, no. 3, pp. 1145-1154, 2009.

[34] J. L. Mathieu, S. Koch, D. S. Callaway, "State estimation and control of electric loads to manage real-time energy imbalance," *IEEE Trans. Power Systems*, vol. 28, no. 1, pp. 430-440, 2013.

[35] B. H. Kim, H. Kim, B. Lee, "Parameter estimation for the composite load model," *Journal of International Council on Electrical Engineering*, vol. 2, no. 2, pp. 215-218, 2012.

[36] F. J. Meyer, K. Y. Lee, "Dynamic power system load modeling by parameter estimation," *Electric power systems research*, vol. 7, no. 3, pp. 231-241, 1984.

[37] R. Teodorescu, F. Blaabjerg, M. Liserre, "Proportional-resonant controllers. A new breed of controllers suitable for grid-connected voltage-source converters," *OPTIM*, Brasov, Romania, 2004.

[38] D. N. Zmood, D. G. Holmes, "Stationary frame current regulation of PWM inverters with zero steady-state error," *IEEE Trans. Power Electronics*, vol. 18, no. 3, pp. 814-822, 2003.

[39] J. Zhang, L. Li, D. G. Dorrell, "Dq coupling suppressed PID controller for the transmission line power flow control using a matrix converter," *In Industrial Electronics Society*, *IECON 2016-42nd Annual Conference of the IEEE*, pp. 6249-6254, 2016.

[40] J. Zhang, D. G. Dorrell, L. Li, Y. Guo, "Decoupling Controller Design and Controllable Regions Analysis for the Space Vector Modulated Matrix Converter-Unified Power Flow Controller in Transmission Systems," *Electric Power Components and Systems*, vol. 46, no. 1, pp. 1-14, 2018.

[41] L. Huber, D. Borojevic, "Space vector modulated three-phase to three-phase matrix converter with input power factor correction," *IEEE Trans. Industry Applications*, vol. 31, no. 6, pp. 1234-1246, 1995.

[42] Z. Malekjamshidi, M. Jafari, D. Xiao, and J. Zhu, "Operation of indirect matrix converters in different SVM switching patterns," *4th IEEE Int. Conf. on Electric Power and Energy Conversion Systems* (*EPECS*), pp. 1-5, 2015.

Jianwei Zhang (S'15) received a B.S. in electrical engineering from the Northwest A&F University, Yangling, Shaanxi, China, in 2014. He received a Ph.D. in electrical engineering from the University of Technology Sydney (UTS), Sydney, New South Wales, Australia, in 2018. From 2015 to 2018, he worked as a Casual Academic at the Faculty of Engineering and IT, UTS. In 2018, he joined Inner Mongolia University of Technology, Hohhot, Inner Mongolia, China.

His research interests include control of power electronic converters, matrix converters, microgrids, and AC motor drives.

Li Li (M'12) was born in Henan, China. He received a B.S. from Huazhong University of Science and Technology in 1996, an M.S. from Tsinghua University in 1999, and a Ph.D. from University of California, Los Angeles in 2005.

From 2005 to 2007, he was a research associate at the University of New South Wales at the Australian Defence Force Academy (UNSW@ADFA). From 2007 to 2011, he was a researcher at the National ICT Australia, Victoria Research Laboratory, Department of Electrical and Electronic Engineering, The University of Melbourne. He joined UTS in 2011 and is currently an Associate Professor. Dr. Li has held several visiting positions at Beijing Institute of Technology, Tsinghua University and UNSW@ADFA. His research interests are control theory and power system control.

David G. Dorrell (M'95–SM'08) is a native of St. Helens, U.K. He received a B.Eng. (Hons.) degree in electrical and electronic engineering from the University of Leeds, Leeds, U.K., in 1988; an M.Sc. degree in power electronics engineering from the University of Bradford, Bradford, U.K., in 1989; and a Ph.D. degree in engineering from the University of Cambridge, Cambridge, U.K., in 1993.

Since 2015, he has been a Professor of Electrical Machines at the University of KwaZulu-Natal, Durban, South Africa. He is also the Director of the EPPEI Specialization Centre of HVDC and FACTS, UKZN. He has held lecturing positions at Robert Gordon University, Aberdeen, U.K., and the University of Reading, Reading, U.K. He was a Senior Lecturer at the University of Glasgow, Glasgow, U.K., for several years. In 2008, he took up a post as a Senior Lecturer at the University of Technology Sydney, Ultimo, NSW, Australia, and he was promoted to an Associate Professor in 2009. He is also an Adjunct Associate Professor with National Cheng Kung University, Tainan, Taiwan. His research interests include the design and analysis of various electrical machines, as well as renewable energy systems.

Dr. Dorrell is a Chartered Engineer in the U.K. and a fellow of the Institution of Engineering and Technology.